RESEARCH ARTICLE SUMMARY

NEUROSCIENCE

Sleep-wake cycles drive daily dynamics of synaptic phosphorylation

Franziska Brüning*, Sara B. Noya*, Tanja Bange, Stella Koutsouli, Jan D. Rudolph, Shiva K. Tyagarajan, Jürgen Cox, Matthias Mann, Steven A. Brown†, Maria S. Robles†

INTRODUCTION: Globally, circadian clock–driven protein phosphorylation is a key mechanism to temporally compartmentalize biological processes across the day in peripheral tissues. In the brain, phosphorylation of several proteins has been reported to correlate with sleep pressure, itself regulated in a circadian fashion. Locally in neurons, phosphorylation plays a critical role in the regulation of synaptic function by allowing rapid modulation of protein activity and could thus dynamically scale synaptic strength in response to circadian or sleep-driven cues. Understanding the magnitude and origin of phosphorylation dynamics within synaptic proteins on a system level would be of great value to mechanistically assess synaptic function deficiencies and to understand temporal contributions to brain pathologies.

RATIONALE: Little is known about whether and how global phosphorylation signaling in synapses is shaped in a time-dependent manner. To comprehensively characterize phosphorylation rhythms in the synaptic compartment driven by circadian and sleep-wake–dependent cues, we biochemically isolated synaptoneurosomes from mouse forebrain and analyzed them with advanced mass spectrometry–based proteomics.

RESULTS: Of more than 8000 phosphopeptides in almost 2000 proteins accurately quantified in the synaptoneurosome compartment across 24 hours, 30% oscillated in abundance. The phases of rhythmic phosphopeptides were distributed in two major clusters, corresponding to the transition from wake to sleep at dawn and sleep to wake at dusk. In addition to important synaptic constituents such as ion channels, receptors, and scaffolds, a large number of kinases were among the synaptic proteins modulated by phosphorylation in a time-dependent manner. More than half of the detected phosphorylated kinases in synapses show rhythmic phosphorylation at one or more residues. Predictive and experimental data demonstrate that widespread dynamic regulation of kinase activity is a core phospho-dependent functional process at synapses. Together, our data uncover molecular processes in synapses whose activity is temporally gated by phosphorylation, such as synaptic inhibition at dawn and excita-

tion at dusk. We further assessed circadian- and sleep-driven signals by interfering with the sleep-wake cycle by applying 4 hours of sleep deprivation at different times of the day. Sleep deprivation resulted in the loss of 98% of rhythmic phosphorylation in forebrain synapses but left circadian cycles unaffected in a core of 41 phosphoproteins that function in synaptic transport and scaffolding.

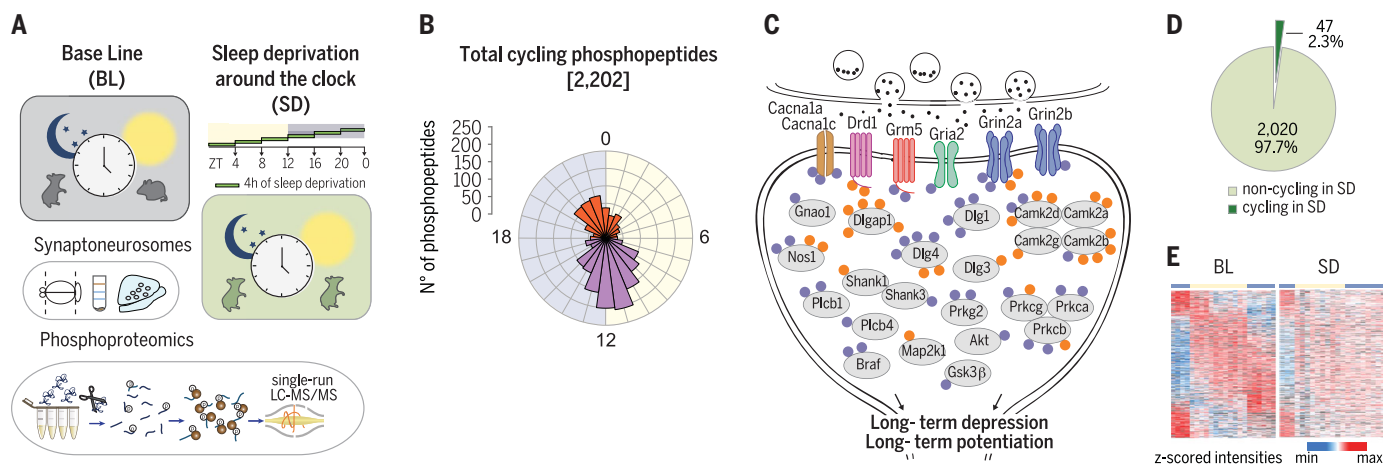Read the full article at http://dx.doi.org/10.1126/science.aav3617

CONCLUSION: This global rhythmic phosphoproteome of isolated synaptoneurosomes reveals a major reorganization of the synaptic molecular compartment concomitant with changes in activity. Our results indicate that phospho-dependent activation of kinases in response to sleep and wake is a core driver of these synaptic phosphorylation dynamics. Together, our data point toward an association of synaptic potentiation with wakefulness (activity) and down-scaling with sleep (rest). High sleep pressure induced through sleep deprivation almost completely abrogates both peaks of daily phosphorylation cycles in synapses. We thus hypothesize that modulation of phosphorylation-mediated synaptic signaling could be a key driver underlying sleep- and wake-dependent mechanisms to regulate synaptic homeostasis and function. ∎

Daily dynamics of global phosphorylation in forebrain synaptoneurosomes under basal and sleep-deprived conditions. (**A**) Quantitative phosphoproteomics analyses of isolated synaptoneurosomes from rested and sleep-deprived mice around the clock. (**B** and **C**) More than 30% of phosphorylations in many synaptic components and numerous kinases cycle daily with peaks at the sleep-wake-sleep transitions. (**D** and **E**) Sleep deprivation abolished 98% of all phosphorylation cycles in synaptoneurosomes.

RESEARCH ARTICLE

NEUROSCIENCE

Sleep-wake cycles drive daily dynamics of synaptic phosphorylation

Franziska Brüning[1,2]*, Sara B. Noya[3]*, Tanja Bange[1], Stella Koutsouli[1], Jan D. Rudolph[4], Shiva K. Tyagarajan[3], Jürgen Cox[4], Matthias Mann[2,5], Steven A. Brown[3]†, Maria S. Robles[1]†

The circadian clock drives daily changes of physiology, including sleep-wake cycles, through regulation of transcription, protein abundance, and function. Circadian phosphorylation controls cellular processes in peripheral organs, but little is known about its role in brain function and synaptic activity. We applied advanced quantitative phosphoproteomics to mouse forebrain synaptoneurosomes isolated across 24 hours, accurately quantifying almost 8000 phosphopeptides. Half of the synaptic phosphoproteins, including numerous kinases, had large-amplitude rhythms peaking at rest-activity and activity-rest transitions. Bioinformatic analyses revealed global temporal control of synaptic function through phosphorylation, including synaptic transmission, cytoskeleton reorganization, and excitatory/inhibitory balance. Sleep deprivation abolished 98% of all phosphorylation cycles in synaptoneurosomes, indicating that sleep-wake cycles rather than circadian signals are main drivers of synaptic phosphorylation, responding to both sleep and wake pressures.

Circadian clocks are endogenous oscillators present in virtually every mammalian cell. The molecular mechanism of the clock drives cycles of transcription, translation, and protein activity to regulate daily changes in physiology and behavior. Mass spectrometry (MS)–based quantitative proteomics has contributed substantially to our understanding of how circadian posttranscriptional mechanisms temporally shape metabolic processes in peripheral tissues (1, 2). Circadian phosphorylation changes by far eclipse the regulation at the transcriptional and proteome levels in amplitude (3). Temporal characterization of proteome and phosphoproteome changes in the central nervous system, by contrast, has been challenging because of the sensitivity, dynamic range, and throughput required to capture the regional, cellular, and synaptic heterogeneity. However, recent advances in MS in combination with spatial isolation methods allow the deep characterization of proteomes from different brain regions and cell populations (4, 5). In addition, high-throughput phosphoproteomic technologies are now suitable for the global characterization of phosphorylation signaling dynamics in different brain areas (6).

Numerous synaptic features—such as diffusion of receptors in membranes, channel conductance, or cytoskeleton remodeling—depend on fast phosphorylation-based control mechanisms. In particular, synaptic plasticity and scaling have been linked to phosphorylation of receptor, scaffolding, cytoskeletal, and other synaptic proteins (7, 8). Although quantitative phosphoproteomics has been applied to the synaptic compartment, technical limitations have so far precluded accurate quantification that would allow the precise characterization of global phosphorylation dynamics associated with synaptic function (7). It is thus unknown whether daily changes in synaptic activity are coupled to global dynamics of phosphorylation in synapses or, moreover, whether daily rhythms of phosphorylation temporally segregate synaptic processes. Two recent reports have addressed these technical limitations by either fractionating postsynaptic density (9) or by mapping whole-brain phosphoproteomics to synaptic protein annotations (10). They highlight a role for sleep pressure in driving synaptic phosphorylation changes associated with the kinase SIK3 (10) and downstream effectors of plasticity such as HOMER1a (9).

We applied state-of-the-art quantitative MS-based proteomics to characterize in vivo phosphorylation dynamics across the day in isolated synaptoneurosomes from mouse forebrain, resulting in the most comprehensive time-resolved phosphoproteome of synapses to date. In combination with in-depth proteomics (11), we found that more than one-fourth of the individual phosphorylation sites in synaptic proteins oscillate daily and independently of protein abundance. Temporally modulated phosphorylation networks gate synaptic processes at both dawn and dusk, primarily dependent on sleep-wake cycles. Thus, maintaining sleep pressure approximately constant across the day leads to a dramatic ablation of global phosphorylation cycles, suggesting a dominant role of both sleep and wake pressure in synaptic phosphorylation dynamics. In turn, our analyses suggest that these dynamics profoundly shape both synaptic function and downstream regulatory networks.

Results

In-depth phosphoproteomic profiling of synaptoneurosomes

To characterize daily dynamics of phosphorylation abundance specifically in synapses, we biochemically isolated synaptoneurosomes from mouse forebrains (11). Mice were kept in 12-hour:12-hour (light:dark) schedules and then euthanized in biological quadruplicates at six time points, every 4 hours, across 24 hours (n = 24 mice). We used a rapid method based on Percoll gradients to prepare synaptoneurosomes from forebrains, containing both pre- and postsynaptic components (12), and immediately flash-froze them to prevent dephosphorylation. To achieve sufficient throughput for our time-dependent experiments, we used the EasyPhos method (13) to enrich phosphopeptides from only 1 mg of protein homogenate for each synaptoneurosome preparation. The MS-based quantitative phosphoproteomics workflow, consisting of single runs on a high-resolution, high-sensitivity quadrupole-Orbitrap HF-X mass spectrometer, is shown in Fig. 1A. Across all samples, this resulted in a total of 10,439 unique phosphosites identified in 14,462 phosphopeptides, mapping to more than 2000 proteins (Fig. 1B and table S1). Comparing phosphorylated amino acids in synapses with our previous circadian study in the liver (3) revealed similar proportions [83.6% phosphoserine (pS), 15.7% phosphothreonine (pT), 0.6% phosphotyrosine (pY)] (Fig. 1B). Phosphopeptide intensities between measurements were highly reproducible in both biological replicates and time points [mean Pearson correlation coefficient (r) = 0.88 and 0.83, respectively] (fig. S1A). The intensities of phosphopeptides in synaptoneurosomes ranged over five orders of magnitude (fig. S1B), similar to what we found in liver, indicating that the synaptic compartment still has a wide quantitative range of phosphorylation levels. To indirectly evaluate our isolation method, we performed a Fisher's exact test on the total phosphoproteome dataset. Of all annotated protein keywords, the top two most significant are "synapse" and "cell junction" (P < 10⁻⁴⁰ for both), and the other highly enriched ones are also relevant to synaptic function, even when analyzing every time point separately (fig. S1, C to E, and materials and methods). Our data

[1]Institute of Medical Psychology, Faculty of Medicine, LMU Munich, Germany. [2]Department of Proteomics and Signal Transduction, Max-Planck Institute of Biochemistry, 82152 Martinsried, Germany. [3]Institute of Pharmacology and Toxicology, Univ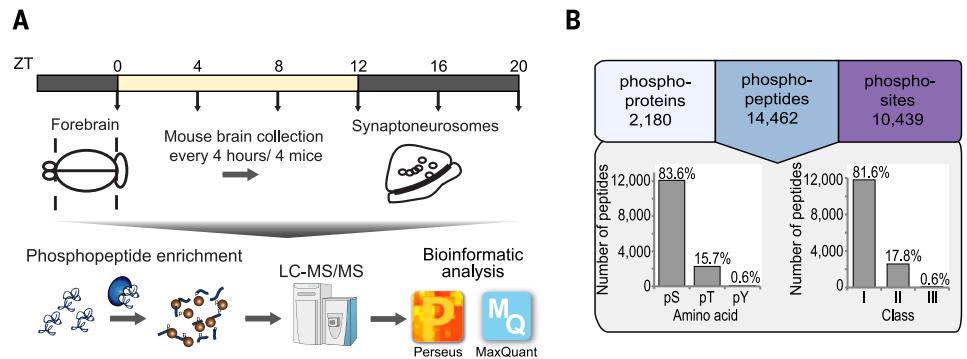ersity of Zurich, Zurich, Switzerland. [4]Computational Systems Biochemistry, Max-Planck Institute of Biochemistry, Martinsried, Germany. [5]Novo Nordisk Foundation Center for Protein Research, Faculty of Health Science, University of Copenhagen, Copenhagen, Denmark.
*These authors contributed equally to this work.
†Corresponding author. Email: charo.robles@med.uni-muenchen.de (M.S.R.); steven.brown@pharma.uzh.ch (S.A.B.)

Fig. 1. Phosphoproteome characterization of synaptoneurosomes isolated across the day from mouse forebrains. (**A**) Experimental workflow. (**B**) Number of identified phosphoproteins, phosphopeptides, and phosphosites in all measured samples. (Bottom left) Distribution of phosphorylated amino acids [serine (pS), threonine (pT), and tyrosine (pY)]. (Bottom right) Number of phosphorylated residues from different classes according to localization probability: class I (probability > 75%), class II (probability = 50 to 75%), and class III (probability < 50%).

show the power of combining high-throughput phosphoproteomics with biochemical isolation of synaptoneurosomes to deeply profile phosphorylation in this discrete neuronal compartment.

Daily rhythms of the synaptic phosphoproteome

Next, we performed statistical cycling analysis in the circadian module of the Perseus software (2, 3, 14) to filter and cosine-fit the phosphopeptide intensities. A total of 2202 (30.4%) of the 7257 phosphopeptides accurately quantified in at least 50% of the samples oscillate in abundance with a rhythm of 24 hours ($q <$ 0.05) (Fig. 2, A and B; table S2; and materials and methods). We detected rhythmic phosphorylations in more than half of the synaptic phosphoproteins (838 out of the total 1655) (Fig. 2C). These cycling sites were localized with high probability to a single residue (mean 0.97), and their amino acid distribution was similar to that of the total dataset (Fig. 1B and fig. S2A). Cycling phosphopeptides had an intensity distribution similar to that of the total phosphoproteome (fig. S2B), implying that circadian phosphoregulation is not biased by abundance. Little is known about the magnitude of dynamic phosphorylation changes in the synaptic compartment, and our data revealed that these changes are substantial: The mean amplitude changes are more than threefold, with hundreds of sites at more than 10-fold (Fig. 2D).

To assess the extent to which these phosphorylation dynamics depend on protein abundance changes, we quantitatively compared the levels of phosphopeptides with the abundance of the corresponding protein. Almost 90% of proteins with cycling phosphopeptides were quantified at the protein level in our companion study (11), and of these, only 5% significantly oscillate in abundance ($q <$ 0.05, period = 24 hours) (Fig. 2E). Even the small fraction of rhythmic proteins with oscillating phosphorylation displays different phases across the day, and furthermore, multiple sites in the same protein generally behaved differently (Fig. 2F and fig. S2C). In

the minor population of rhythmic proteins carrying cycling phosphorylation, the mean amplitudes at the phosphorylation level were 10-fold larger than those at the protein level (Fig. 2G). Our data clearly establish that protein phosphorylation in forebrain synaptoneurosomes is highly dynamic across the day and almost completely independent of protein abundance, suggesting another layer of synaptic functional regulation.

Temporal compartmentalization of synaptic protein phosphorylation

Our previous study in liver revealed that dynamic phosphorylation drives daily organ functions to a previously unappreciated degree (3). Examining the phosphorylation rhythms in the synaptic compartment showed that the phases of rhythmic phosphopeptides gathered in two distinct clusters. The larger one, at the light-to-dark transition when mice start to be active, contains two-thirds of the phosphopeptides, whereas the remaining ones peak at the end of the night, preceding the sleep phase (Fig. 3A). This phase distribution indicates a major rewiring of protein phosphorylation and presumably synaptic function at the wake-to-sleep and sleep-to-wake transitions. In order to identify synaptic functions that are temporally compartmentalized by protein phosphorylation, we searched for statistically enriched protein annotations in each of the two defined phase clusters (Fisher's exact test, $P <$ 0.05) (materials and methods). At the end of the resting phase, our analysis found keywords corresponding to "cell adhesion" and "cell junction" as well as "ion channels," "ion transporters," "hydrolases," and "kinases highly enriched." By contrast, "cell projection," "cytoskeleton," and "ubiquitin conjugation protein" annotations are overrepresented in the phosphopeptide cluster at the end of the activity phase (Fig. 3, B and C, and table S3). Proteins involved in cell division and mitosis were also enriched in the phosphorylation cluster at the end of the activity phase, likely because several cell cycle kinases, such as CDK5, are also important for synaptic activity (15). Thus, our

results imply that different remodeling processes that are known to occur at synapses (16) might occur separately in temporally distinct nodes.

Synapses are hubs of kinases

We next focused our attention on the major and specific enrichment of kinases, key regulators of almost all cellular processes, in the phosphopeptide cluster that peaks at the end of the resting phase. We identified almost 500 phosphorylated peptides from a total of 128 kinases from all major families in mammals. Thus, a fifth of the total mouse kinome is not only present in the synaptic compartment but also detectable in a phosphorylated form (fig. S3A). More than half of these kinases show at least one rhythmic phosphorylation ($q <$ 0.05) (Fig. 4, A and B, and table S4), and these belong to all major kinase families, with a higher representation of AGC threonine/serine kinases (Fig. 4, C and D). All of the 66 kinases with rhythmic phosphorylation were also quantified at the protein level in the synaptic compartment (11); however, only four of them cycled in protein abundance (fig. S3B). Therefore, phosphorylation, rather than protein abundance, likely regulates temporal kinase function at synapses across the day. Our analyses also detected cycles of phosphorylation and protein abundance in several phosphatases at the synapses but in a lesser extent compared with kinases. Out of the 77 phosphatases detected in synapses, only three cycle at the protein level, and 10 out of 20 phosphorylated phosphatases showed rhythms of phosphorylation (fig. S4, A to D).

The overall phase distribution of rhythmic phosphopeptides from kinases resembles the total cycling synaptic phosphoproteome (Figs. 3A and 5A), suggesting that phosphorylation-dependent temporal activation of kinases contributes to the global phosphorylation rhythms in synapses. However, because site-specific phosphorylation does not always imply changes in kinase activity, we next set out to identify temporally activated kinases with an unbiased workflow that uses high-confidence protein-
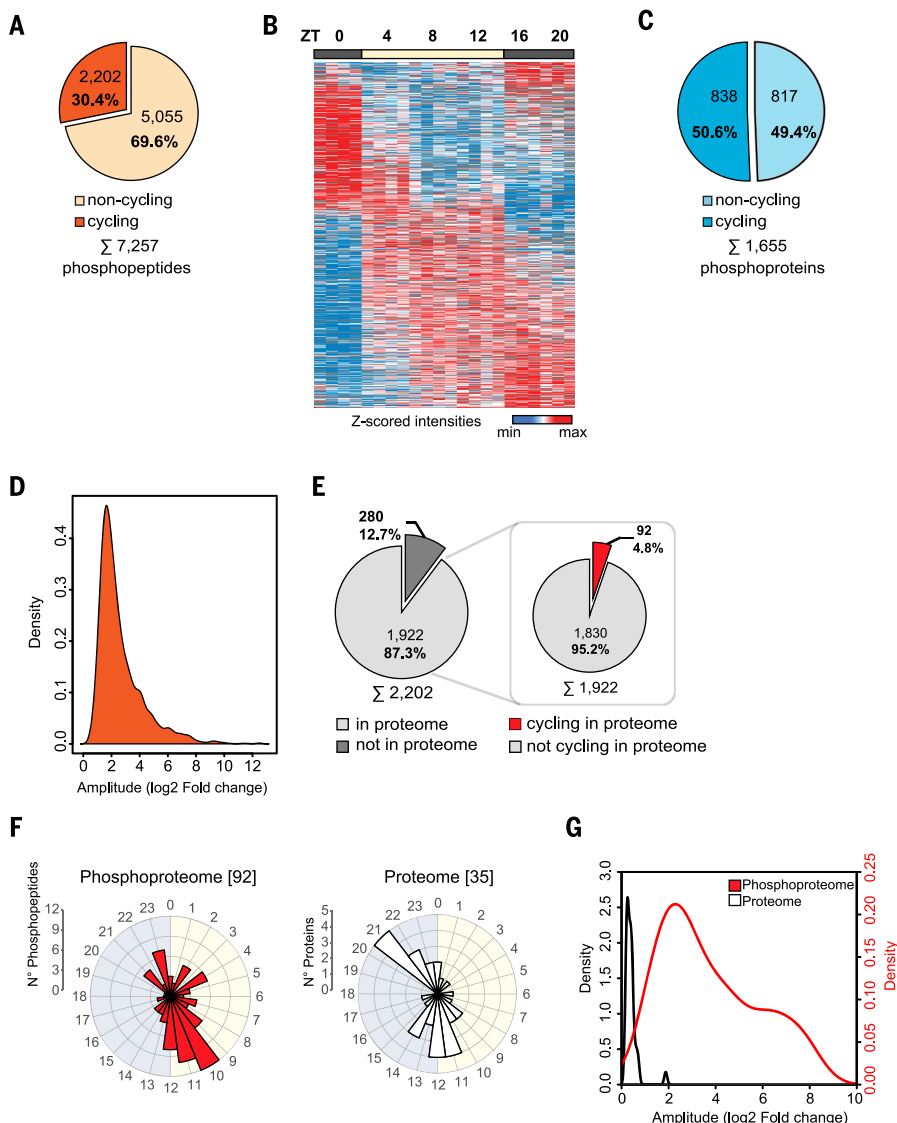
Fig. 2. Daily rhythms of the synaptic phosphoproteome. (**A**) Pie chart showing the percentage of phosphopeptides oscillating ($q < 0.05$, period = 24 hours) in synaptoneurosomes. (**B**) Heat map with the intensities (log2 z-scored normalized) of each cycling phosphopeptide (rows) across the measure samples (columns) ordered by peak of abundance. (**C**) Pie chart with the percentage of proteins carrying at least one cycling phosphorylation in synaptoneurosomes. (**D**) Density plot showing the calculated amplitudes of rhythmic phosphopeptides in synaptoneurosomes. (**E**) Pie charts showing (left) the percentage of cycling phosphopeptides from proteins quantified in our proteome study and (right) the fraction of cycling phosphopeptides in proteins that are also rhythmic at the protein level. (**F**) Rose plots representing the phase distribution of rhythmic phosphopeptides (left) and their corresponding oscillating proteins (right). (**G**) Density plots comparing the amplitudes of the rhythmic phosphopeptides and the corresponding oscillating proteins.

protein interaction networks and large-scale phosphorylation data to retrieve protein signaling functionality. This PHOTON pipeline assigns a score to each protein according to the phosphorylation status of their interacting proteins (*17*). Because these scores reflect the changes in phosphorylation levels of their substrates and interactors, kinases that are activated rather than only phosphorylated should have PHOTON scores that cycle across the 24 hours, with the maximum score indi-

cating the peak of kinase activity. From the 66 synaptic kinases with rhythmic phosphorylation, this analysis resulted in rhythmic activity patterns for 13 of them (materials and methods). Of these, 11 are active at the sleep-wake transition, including protein kinase C (PRKCA, PRKCB, and PRKCG) and Ca²⁺/calmodulin-dependent kinase 2 (CAMK2B and CAMK2G). Conversely, the tyrosine-protein kinase ABL2 and the serine/threonine-protein kinase DCLK1 showed the opposite behavior, peaking in

activity at the wake-sleep transition (Fig. 5, B and C).

To substantiate the PHOTON prediction data, we used a second computational method [kinase substrate enrichment analysis (KSEA)] that infers kinase activity by using curated kinase-substrate relationships (*18*). This second method estimated, very similarly to PHOTON, the activation of PKC and CAMK2 at the sleep-wake transition (fig. S5 and materials and methods). We verified these kinase activity patterns by immunoblotting using phospho-specific antibodies against phosphorylated residues known to regulate the activity of these two kinases (fig. S6, A and B) (*19, 20*). The KSEA algorithm also identified additional putative temporally activated kinases with rhythms of phosphorylation (fig. S5). For example, this method predicted that GSK3β, a molecular switch in synaptic activation and plasticity (*21*), is active during the sleep stage. Such predicted activation would be in antiphase to the phosphorylation cycle of two residues known to inhibit its kinase activity, S389 and S9 (*22, 23*). The former was detected in our data with a peak at ZT11, and the latter was further confirmed by means of immunoblotting (fig. S6C).

Considering the published literature about rhythmically regulated kinases predicted by PHOTON and KSEA, the kinases activated at the transition to the wake phase (CAMK and PKC) are associated with excitatory synaptic activity (*8*), whereas those activated at the transition to and during the sleep phase (ABL2, DCLK1, and GSK3β) are associated with inhibitory synaptic activity (*24, 25*). An identical temporal compartmentalization of synaptic function was independently predicted by PHOTON by means of phosphorylation dynamics of Gene Ontology (GO) molecular functions (materials and methods); it inferred that the triggering of inhibitory synaptic mechanism, involving γ-aminobutyric acid (GABA), occurs at the end of the wake period, whereas glutamate-mediated synaptic excitatory activity was predominantly associated to the sleep-wake transition (fig. S7). These data are consistent with the roles of these synaptic types in sleep and wake, respectively (*26, 27*).

Sleep deprivation abrogates synaptic phosphorylation rhythms

We hypothesized that the sharp biphasic distribution of synaptic phosphorylation patterns at the wake-sleep and sleep-wake transitions might reflect either buildup and dissipation of sleep pressure (a sleep homeostat), or alternatively a circadian (time-of-day) mechanism, or a combination of the two. To test their relative contributions, we subjected mice to 4 hours of sleep deprivation (SD) by means of gentle handling (*28*) before each time point
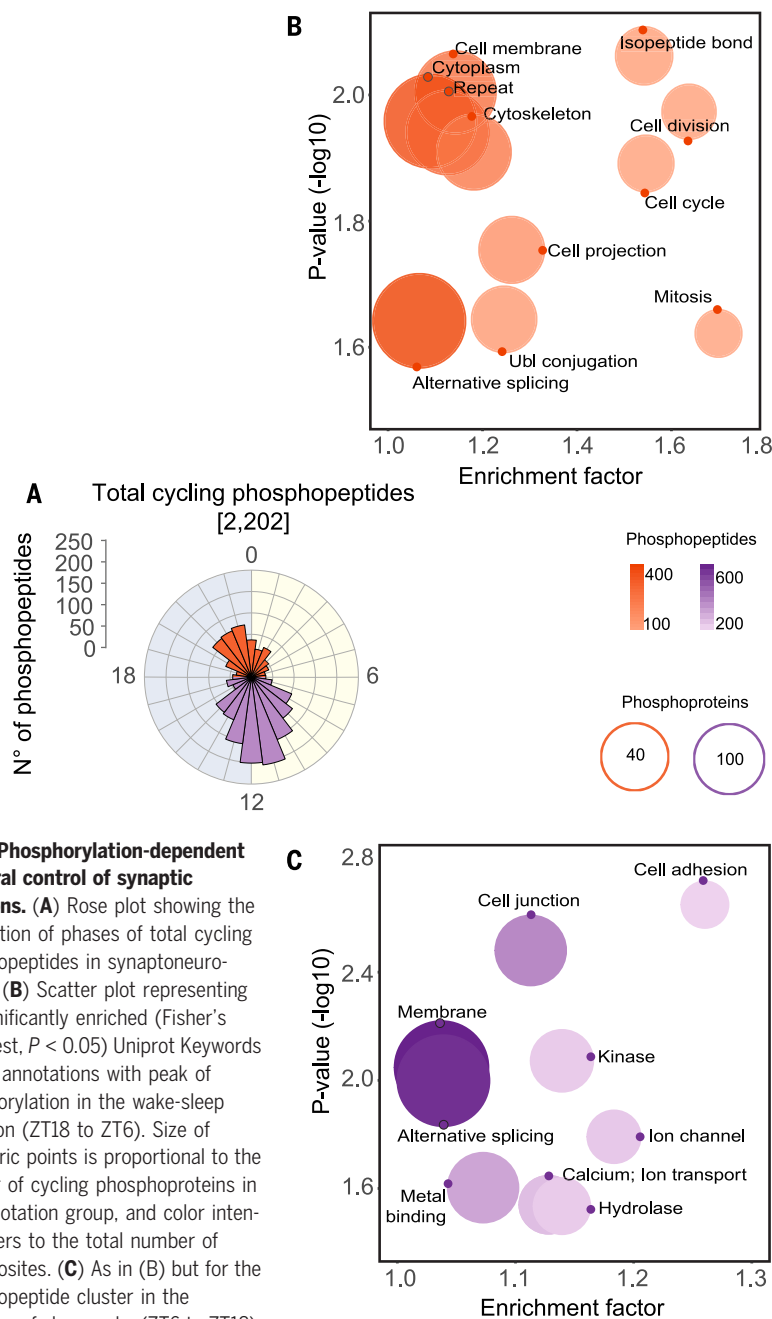
Fig. 3. Phosphorylation-dependent temporal control of synaptic functions. (**A**) Rose plot showing the distribution of phases of total cycling phosphopeptides in synaptoneurosomes. (**B**) Scatter plot representing the significantly enriched (Fisher's exact test, $P < 0.05$) Uniprot Keywords protein annotations with peak of phosphorylation in the wake-sleep transition (ZT18 to ZT6). Size of geometric points is proportional to the number of cycling phosphoproteins in the annotation group, and color intensity refers to the total number of phosphosites. (**C**) As in (**B**) but for the phosphopeptide cluster in the transition of sleep-wake (ZT6 to ZT18).

and collected brains every 4 hours in 24 hours ($n = 4$ brains per time point) (Fig. 6A). A similar protocol of SD across the 24-hour time course equalizes sleep pressure to keep it constantly high (29). First, we empirically verified that this was the case by measuring the amplitude of electroencephalogram (EEG) oscillations during sleep (0.5 to 4 Hz, the "delta" range proportional to sleep pressure) (30) and demonstrating that this was similar at each time point to that maximally observed spontaneously in the day before the manipulation. Although some fluctuation in delta power across time points was still observed, we estimated it to be less than a fifth of what is

observed under the same conditions across the normal circadian day. We also demonstrated that the pattern and timing of sleep and activity in the subsequent day were not altered by this protocol—that the protocol was not shifting the phase of the circadian clock (Fig. 6B and figs. S8, A and B, and S9). Next, we prepared synaptoneurosomes from forebrains of SD mice, and as in baseline (BL) conditions, we enriched phosphopeptides before MS analysis (Fig. 6A and materials and methods). We accurately quantified 7021 phosphopeptides in at least 50% of the samples, which are very similar values to those in the BL experiment, with more than 90% (6526

phosphopeptides) overlap between them (fig. S10A). Cycling analysis of the 6526 phosphopeptides revealed almost complete abrogation of rhythmic phosphorylation in the synaptic compartment of SD mice. Only 2.3% (47 phosphopeptides corresponding to 41 proteins) of the phosphopeptides rhythmic in BL maintained the cycle in SD (period = 24 hours, $q < 0.05$) (Fig. 6, C and D; table S5; and materials and methods). These few remaining cycling phosphopeptides oscillated with similar amplitudes and with comparable phases in both conditions (Fig. 7, A to C, and table S6), suggesting that they might be driven primarily by the circadian clock. Of the corresponding 41 synaptic phosphoproteins, 31 belong to interconnected cellular structures such as cytoskeleton, synaptic scaffolding, membrane, vesicle trafficking, and ubiquitin mechanisms, all of which are important for synaptic integrity and function (fig. S11) (31–33). Aside from this small fraction, the remaining 98% of phosphorylations, affecting all aspects of synaptic biology, were severely affected by SD across the day, leading to a dramatic loss in rhythmicity (fig. S10, B to D).

Discussion

Synaptic plasticity and function dynamically change across the day (34). It is already known that changes in synaptic activity are associated with the phosphorylation of several signaling proteins (8, 33). However, our large-scale quantitative phosphoproteome of isolated synaptoneurosomes resulted in a comprehensive time-resolved map of synaptic phosphorylation across the entire wake and sleep phases. The phosphoproteome is much more dynamic than the proteome (50% of synaptic proteins showing cyclic phosphorylation at one or more sites versus only 12% of synaptic proteins whose abundance oscillates). Moreover, similar to our previous finding in the liver (3), mean fold-changes of the phosphoproteome are more than threefold higher than in the proteome. At 7000 accurately quantified phosphopeptides, our analysis allowed in-depth bioinformatic analysis, retrieving both known and unknown temporally regulated processes at synapses. Overall, the phases of cycling phosphorylation fall into two main clusters just preceding daily activity-rest transitions, when the mouse typically wakes up or falls asleep, implying a major role of synaptic phosphorylation in regulating these transitions. This pattern contrasts markedly with that of the rhythmic phosphoproteome of total forebrain (including entire cells, not just synapses), where phosphorylation peaks gather at the wake and sleep periods (fig. S12), similarly to what we observed for the total rhythmic forebrain proteome described in (11).

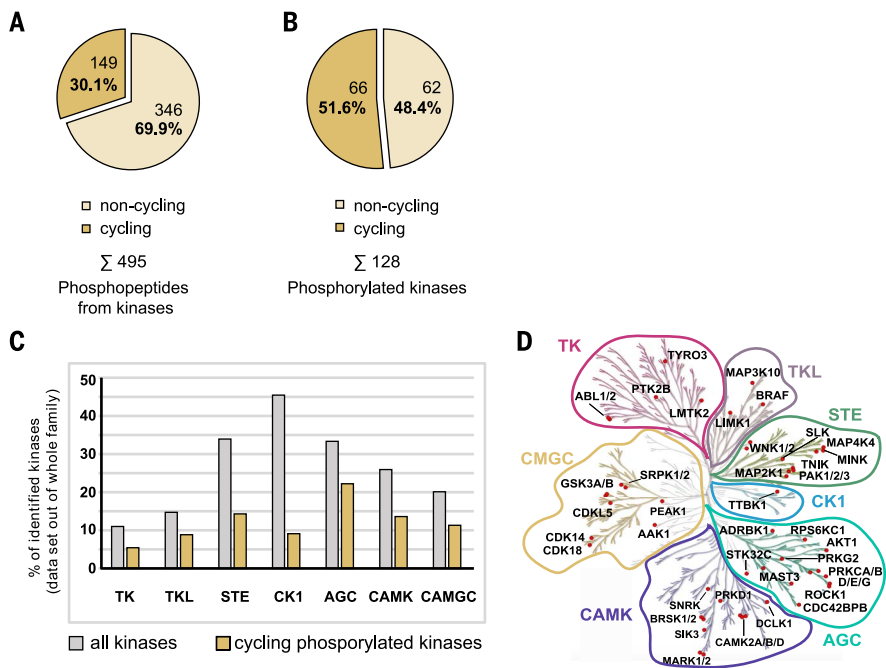Numerous kinases are expressed in the brain, and some of them also have been localized

Fig. 4. Synapses are hubs of kinases. (**A**) Pie chart showing the percentage of cycling and not cycling phosphopeptides from kinases. (**B**) Pie chart showing the percentage of kinases with at least one cycling and noncycling phosphorylation. (**C**) Bar plot representing the percentage of all (gray) and cycling (orange) phosphorylated kinases quantified in synaptoneurosomes from each of the major mammalian kinase families. (**D**) Kinases with at least one cycling phosphorylation annotated to the major kinase families (52 out of the total 66 cycling) using www.kinhub.org. TK, tyrosine kinases; TKL, tyrosine kinase-like; STE, homologs of the yeast *STE7*, *STE11*, and *STE20* genes; CK1, casein/cell kinase 1 family; AGC, protein kinase A, G, C families; CAMK, calmodulin/calcium-regulated kinases and some non–calcium-regulated families; and CMGC is CDK, MAPK, GSK3, and CLK kinase families. Atypical kinases are not shown.

to the synaptic compartment (*35*). However, our study clearly identifies the synapse as a major kinase hub. We detected more than 100 phosphorylated kinases (20% of the total kinome) and found that 50% show daily rhythmic phosphorylation of least one residue. Combining protein interaction network data with our quantitative phosphoproteome revealed that these phosphorylation changes regulate the activity of at least a subset of them, predictions that we verified through immunoblotting of known activating and inhibiting phosphoresidues for some kinases. Prediction and empirical validation of kinase activities notably matched to the phosphorylation profiles of known substrates detected in our dataset (fig. S6). Although the existing network data are sufficient to associate rhythmic activity with a substantial subset of the kinases, more complete networks and meta-analyses will likely establish activity changes for a much larger fraction of the cycling synaptic phosphoproteome in the future. Together, the combination of predictive and experimental data places extensive temporal regulation of kinase activity as a core phospho-dependent functional process at the synapse.

An obvious question leading from these data concerns the regulatory target of this con-

trol. Considering our predictive and experimental data, we speculate that one possible consequence could be temporally distinct windows for promotion of synaptic long-term potentiation (LTP) and long-term depression (LTD). Kinases with higher activity in anticipation of the wake period are involved in LTP, such as CAMK2 and PRKC, which function directly downstream of *N*-methyl-D-aspartate receptor (NMDAR) Ca²⁺ signaling (*8*). By contrast, ABL2 and DCLK1, two kinases that modulate structural synaptic plasticity (*24*, *25*), peak in activity in anticipation of sleep. Lack of ABL2 leads to elevated NMDAR synaptic currents (*25*); therefore, ABL2 activation at the beginning of the resting phase may mediate synaptic down-scaling. Moreover, phospho-dependent activation of GSK3β during sleep regulates LTD and GABA receptor (GABAR) trafficking (*21*), and its activity is in turn blocked at the wake transition by LTP-mediated phosphorylation of its inhibitory site S9 (*36*) and S389. This mechanistic speculation is further supported by the extensive overlap of phosphorylated residues increased by LTP induction in mouse hippocampus (*33*) with those peaking at the transition to the wake phase in our dataset (fig. S13). Together, our data point toward an association of synaptic potentiation

with wakefulness (activity) and synaptic down-scaling with sleep (rest). This supports the general synaptic homeostasis hypothesis for sleep—that synaptic down-scaling is a key function of sleep (*37*) at the molecular level—and provides starting points for a multitude of mechanistic investigations.

Critically, this functional support is created both by phosphorylation rhythms dependent on the sleep-wake cycle and their peaks clustering at the wake-sleep-wake transitions. Thus, an experimental protocol to produce constant sleep pressure across the 24-hour day almost entirely abrogates global diurnal oscillation of phosphorylation in the synaptic compartment. This discovery establishes the importance of the homeostatic regulation of sleep over any other mechanism in generating daily rhythms of phosphorylation to modulate synaptic function. However, these phosphorylation changes are governed both by wake and by sleep. A recent analysis of wake-dependent protein phosphorylation in total mouse brain showed that increasing hours of SD resulted in increasing average phosphorylation levels of 80 synaptic proteins (*10*). We examined our data and found phosphorylations in all of those 80 proteins, with sites showing increased phosphorylation at times of high sleep pressure in 69 of them. However, our amino acid–resolution data reveal a more nuanced picture than a simple overall increase in phosphorylation, with both sleep- and wake-dependent phosphorylation at different residues in these proteins. Another recent phosphoproteomics study in the synaptic compartment showed that sleep regulates dephosphorylation of AMPA receptors in response to HOMER1a-dependent immediate early transcriptional signaling (*9*). Our data independently support these findings, extend them to several other neurotransmitter receptors, and supply their diurnal rhythms of phosphorylation in response to sleep and wake pressure. Globally across the entire phosphoproteome, we found about one-third of cycling phosphorylations to be maximal at the end of the wake phase when sleep pressure is highest and two-thirds to peak at the end of the sleep phase before waking.

Although the vast majority of protein phosphorylation appears to be regulated by sleep or wake states, a small number of rhythmic phosphorylations remain unchanged in amplitude and phase under SD. These phosphorylations occur in a highly connected node of proteins involved in both synaptic vesicle trafficking (molecular motors and microtubule-associated proteins) and synaptic scaffold (SHANK3, PICCOLO, and BASSOON). Circadian regulation of cortical function is already well documented at both behavioral and molecular levels (*38*). Our data imply that even as sleep-wake pressures dynamically reconfigure
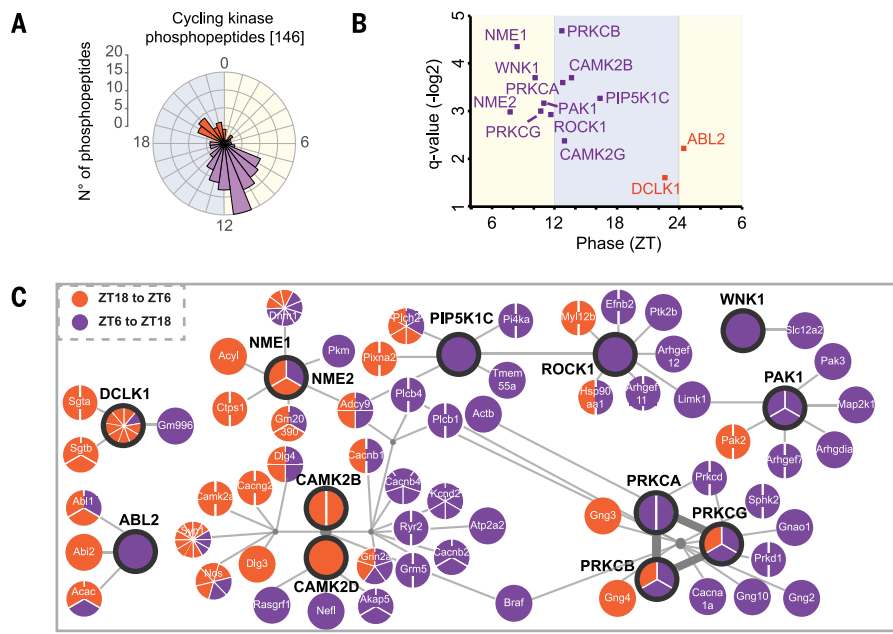
Fig. 5. Rhythmic phosphorylation and activation of synaptic kinases. (**A**) Rose plot with the phases of cycling phosphopeptides from kinases detected in synaptoneurosomes. Colors denote the clusters of wake-sleep transition (ZT18-ZT6, orange) and sleep-wake transition (ZT6-ZT18, purple). (**B**) Scatter plot showing kinases temporally activated predicted by PHOTON. The x axis indicates the phase of activation, and the y axis indicates the q value of the cycling analysis by using PHOTON scores. Kinase names are color-coded according to the two phosphopeptide clusters shown in (A). (**C**) Protein interaction network of PHOTON predicted cycling active kinases (q < 0.05) with rhythmic phosphorylations with their cycling phosphorylated interactors. Nodes are divided on the basis of the number of cycling phosphorylations identified in each protein and color-coded according to the clusters in (A). Nodes with thick lines denote those kinases with rhythmic phosphorylated residues that are also predicted to be temporally activated by PHOTON.

synaptic structure and function, circadian control—or at least circadian clock-sleep interactions—continue to influence cortical function. For example, in our accompanying manuscript, we show that synaptic provisioning of RNA can be independently controlled by the circadian clock or by sleep-circadian interactions (*11*). For both synaptic protein abundance and synaptic protein phosphorylation, however, by far the major diurnal influence is that of daily sleep and wake. The mechanism of this influence remains unknown and could include not only direct signaling (such as receptor-driven kinase cascades) but also indirect effects such as light-dark cycles or changes in cortisol or body temperature, which have been shown to play roles in sleep-wake–dependent gene expression (*39*) and in circadian entrainment (*40, 41*).

This study presents in vivo proof of rhythmic orchestration for thousands of phosphorylation events in synapses across the day. Our study demonstrates a central role for sleep-wake cycles in phosphorylation-dependent regulation of many aspects of synaptic function in response to both sleep and wake pressure, potentially modulating processes that range from plasticity to cellular house-

keeping. Interfering with rest-activity cycles almost completely abolished rhythms of phosphorylation in synaptic proteins. Our findings may thus contribute to understanding the molecular basis of mental dysfunction frequently associated with SD.

Materials and methods
Animals and tissue collection

All experiments were performed in accordance with the Animal Welfare Officer of the University of Zürich and the veterinary authorities of the Canton of Zürich. For the circadian base line (BL) experiments, 10-week-old male C57BL/6 mice were housed with free access to food and water and entrained to a 12-hour/12-hour light-dark schedule for 14 days. Mice were sacrificed at 4-hour intervals over 1 day. At the time points overlapping with light transitions (ZT0 and ZT12), euthanasia was performed by cervical dislocation before the light change. For the around-the-clock SD, mice were allowed to acclimatize to a 12-hour light/12-hour dark cycle for 14 days. Six groups of mice were sleep deprived for 4 hours by gentle handling (cage exchange and introduction of novel objects) before being sacrificed at different times of day (ZT0, ZT4,

ZT8, ZT12, ZT16, and ZT20). Animals were sacrificed by cervical dislocation avoiding anesthetics, which are potent inhibitors of synaptic transmission. In addition, to boost preservation of phosphorylation, total preparation time was minimized, and samples were kept cooled at every step of the protocol.

Electroencephalogram (EEG) recording and sleep data analysis

Adult wild-type (WT) mice were used for surgery (8 to 10 weeks old at surgery). Mice were implanted epidurally under isoflurane anesthesia for EEG recording. Right before and 24 hours after surgery mice were treated with an analgesic (Temgesic, 0.1 mg/kg, intraperitoneal). Gold-plated miniature screws (0.9 mm diameter) were used as EEG electrodes and positioned on the left hemisphere above the frontal cortex (1.5 mm anterior to bregma, 1.5 mm lateral to the midline) and the parietal cortex (2 mm posterior to bregma and 2 mm lateral to the midline). The reference electrode was placed above the cerebellum (2 mm posterior to lambda, 0 mm lateral to the midline). Screws were connected to copper wires and fixed to the skull with dental cement (Paladur 2-component system). Electromyography (EMG) was recorded using two gold wires (0.2 mm diameter) inserted bilaterally in the neck muscle. After 1 week of recovery EEG-EMG was recorded continuously for 7 days. 2 cohorts of 6 and 8 mice, respectively, underwent a BL days recording and 3 SD days with 48 hours of recovery in between. Cohort 1 underwent SD at ZT4-8, ZT12-16 and ZT 16-20. Cohort 2 underwent SD at ZT0-4, ZT8-12 and ZT20-24. SD was performed by gentle handling as described by (*42*). Both EEG and EMG signals were amplified (factor 2000), analog filtered (high-pass filter: –3 dB at 0.016 Hz; low-pass filter: –3 dB at 40 Hz, less than –35 dB at 128 Hz), sampled with 512 Hz, digitally filtered (EEG: low-pass FIR filter 25 Hz; EMG: band-pass FIR 20-50 Hz) and stored with a 128 Hz resolution. EEG power spectra were computed for 4-s epochs by a Fast Fourier Transform routine within the frequency range of 0.5 to 25 Hz. Between 0.5 Hz and 5 Hz, 0.5 Hz bins were used, and between 5 and 25 Hz 1 Hz bins were used. The corresponding slow-wave-activity (SWA) was calculated using the raw parietal and frontal EEG, as well as the raw and integrated EMG to visually score three vigilance states [non–rapid eye-movement (NREM) sleep, rapid eye-movement (REM), and wake] for 4-s epochs. Epochs containing artifacts were identified and excluded from the spectral analysis. Data analysis was carried out using MATLAB version R2015a (The Math Works, Natick, MA, USA). Relative frontal SWA was calculated relative to the mean SWA at ZT8-12 during the BL day. Sleep loss was calculated
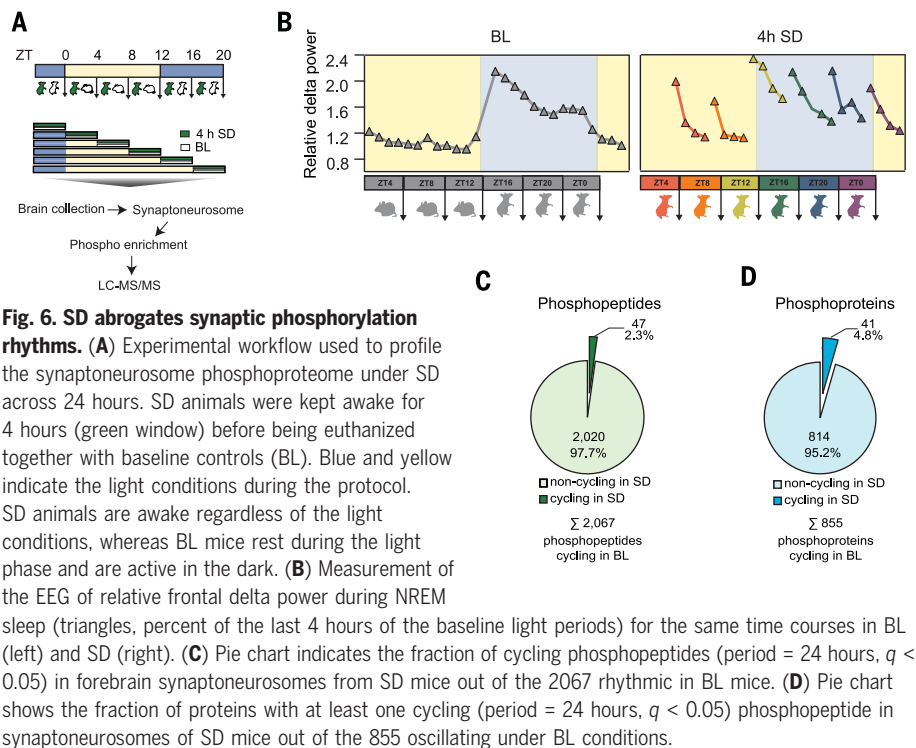
Fig. 6. SD abrogates synaptic phosphorylation rhythms. (**A**) Experimental workflow used to profile the synaptoneurosome phosphoproteome under SD across 24 hours. SD animals were kept awake for 4 hours (green window) before being euthanized together with baseline controls (BL). Blue and yellow indicate the light conditions during the protocol. SD animals are awake regardless of the light conditions, whereas BL mice rest during the light phase and are active in the dark. (**B**) Measurement of the EEG of relative frontal delta power during NREM sleep (triangles, percent of the last 4 hours of the baseline light periods) for the same time courses in BL (left) and SD (right). (**C**) Pie chart indicates the fraction of cycling phosphopeptides (period = 24 hours, $q <$ 0.05) in forebrain synaptoneurosomes from SD mice out of the 2067 rhythmic in BL mice. (**D**) Pie chart shows the fraction of proteins with at least one cycling (period = 24 hours, $q < 0.05$) phosphopeptide in synaptoneurosomes of SD mice out of the 855 oscillating under BL conditions.

by comparing NREM sleep amount in each 4h SD slot to the sleep amount in the same time of day of the corresponding BL day [1-way analysis of variance (ANOVA), $P < 0.05$]. Sleep latency was analyzed by measuring the time each mouse stayed awake after the end of each 4 hours SD until it slept for more than 1 min (1-way ANOVA, $P < 0.05$).

Purification of synaptoneurosomes

Synaptoneurosomes and total mouse forebrain samples were prepared as described previously (*12*). In brief, brain was isolated and rapidly cooled to 4°C, washed in ice-cooled sucrose buffer (320 mM Sucrose, 5 mM HEPES, pH 7.4) followed by homogenization with a Teflon-glass tissue grinder using a motor-driven pestle keeping samples cooled. To isolate synaptoneurosomes, each forebrain homogenate was centrifuged at 1000 g for 10 min. 2 ml of the supernatant were loaded over discontinuous Percoll gradients (3%, 10%, and 23% Percoll in sucrose buffer) and centrifuged at 31,000 g for 5 min. The fraction at the interfaces between 3-10% and 10 to 23% were collected and further centrifuged at 20,000 g to pellet synaptoneurosomes. All centrifugation steps were performed at 4°C. All solutions were supplemented with complete protease inhibitor cocktail (Roche), 0.05 mM DTT, 0.1 mM PMSF and RNaseOUT 20 U/10 μl (Invitrogen).

Sample preparation and phosphopeptides enrichment

Isolated synaptoneurosome and total forebrain samples were lysed [0.1 M Tris-HCl (pH 7.6) and 4% SDS], sonicated in a bioruptor (4°C for 15 min or until homogenous suspension was formed) and boiled at 95°C for 5 min. A total of 1 mg protein lysate was treated first with 1 μl DTT (1 M) followed by 10 μl 2-Chloroacetamide (0.5 M). Each treatment was performed at room temperature (RT; 22°C) for 20 min. The lysates were precipitated with acetone and phosphopeptides were enriched using the EasyPhos method as described (*3*). In detail, pellets were resuspended in 500 μl trifluoroethanol (TFE) buffer prior to the addition of digestion enzymes (trypsin and LysC) 1:100 (protein:enzyme). After overnight incubation at 37°C with rapid agitation (1500 rpm) 150 μl 3.2 M KCl, 55 μl of 150 mM KH$_2$PO$_4$, 800 μl 100% acetonitrile (ACN), and 95 μl 100% trifluoroacetic acid (TFA) were added to the peptides and incubated at RT for 5 min at 1600 rpm prior to centrifugation. The peptide supernatant was transferred to a clean 2 ml tube, TiO$_2$ beads subsequently added at a ratio of 10:1 beads/protein, and incubated at 40°C for 5 min at 2000 rpm. Beads with bound phosphopeptides were pelleted by centrifugation for 1 min at 3500 g and the supernatant was discarded. Beads were then resuspended in wash buffer (60% ACN and 1% TFA) and transferred to a clean 2 ml tube, and washed further four times with 1 ml of washing buffer. After the last wash, beads were resuspended in transfer buffer (80% ACN and 0.5% acetic acid) and transferred on top of C8 (3M Empore) StageTips. Phosphopeptides were eluted with 60 μl elution buffer [40% ACN and 15% NH4OH (25%, HPLC grade)] and collected in clean PCR

tubes, concentrated in a SpeedVac for 15 min at 45°C, and acidified with 10 μl of 10% TFA. Peptides were then desalted using StageTips with two layers of styrenedivinylbenzene–reversed phase sulfonated (SDB-RPS; 3M Empore), washed twice with wash buffer (0.2% TFA) and once with isopropanol containing 1% TFA. Peptides were eluted by adding 60 μl SDB-RPS elution buffer [80% ACN, 1.25% NH4OH (25%, HPLC grade)] and immediately concentrated in a SpeedVac for 30 min at 45°C. Concentrated peptides were then resuspended in a buffer containing 2% ACN and 0.1% TFA prior to LC-MS/MS analysis.

LC-MS/MS analysis and data processing

Phosphopeptides were loaded onto a 50 cm reversed-phase column (diameter 75 μM; packed in-house with 1.9 μM C18 ReproSil particles [Dr. Maisch GmbH]). The temperature of the column oven was maintained at 60°C. The column was mounted to an EASY-nLC 1200 system (Thermo Fisher Scientific). The peptides were eluted with a binary buffer system consisting of buffer A (0.1% formic acid) and buffer B (80% ACN and 0.1% formic acid). A gradient length of 140 min was chosen (5 to 65% buffer B for 130 min followed by 10 min 80% buffer B) with a flow rate of 300 nl/min. Peptides were analyzed in a Q Exactive HF (synaptoneurosomes) and Q Exactive HF-X (total forebrain) mass spectrometer (MS) (Thermo Fisher Scientific) coupled to the nLC. Full scans [300 to 1600 mass/charge ratio (m/z), $R = 60,000$ at 200 m/z] were obtained at a target of 3e6 ions. The 10 most abundant ions were selected and fragmented with higher-energy collisional dissociation (HCD) (target 1e5 ions, maximum injection time 120 ms, isolation window 1.6 m/z, normalized collision energy 25% underfill ratio 40%) followed by the detection in the Orbitrap ($R = 15,000$ at 200 m/z). Raw MS data files were processed using MaxQuant [version 1.5.5.6 and 1.5.5.12 (*43*)] with the Andromeda search engine using false discovery rate (FDR) < 0.01 at protein, peptide, and modification level. The default settings were used with the following modifications: (i) the variable modification methionine (M), acetylation (protein N-term), as well as phosphorylation (STY) and the fixed modification carbamidomethyl (C) were selected, (ii) only peptides with a minimal length of seven amino acids were considered, and (iii) the "match between run" option was enabled with a matching time window of 0.7 min. For protein and peptide identification we used the UniProt database from mouse (September 2014) containing 51,210 entries. Each raw file was treated as one experiment. The following samples were not considered for the final analysis due to low identification number and outlier clustering within the replicates: replicate 4 of ZT16, 3 of ZT20 of the base line group and
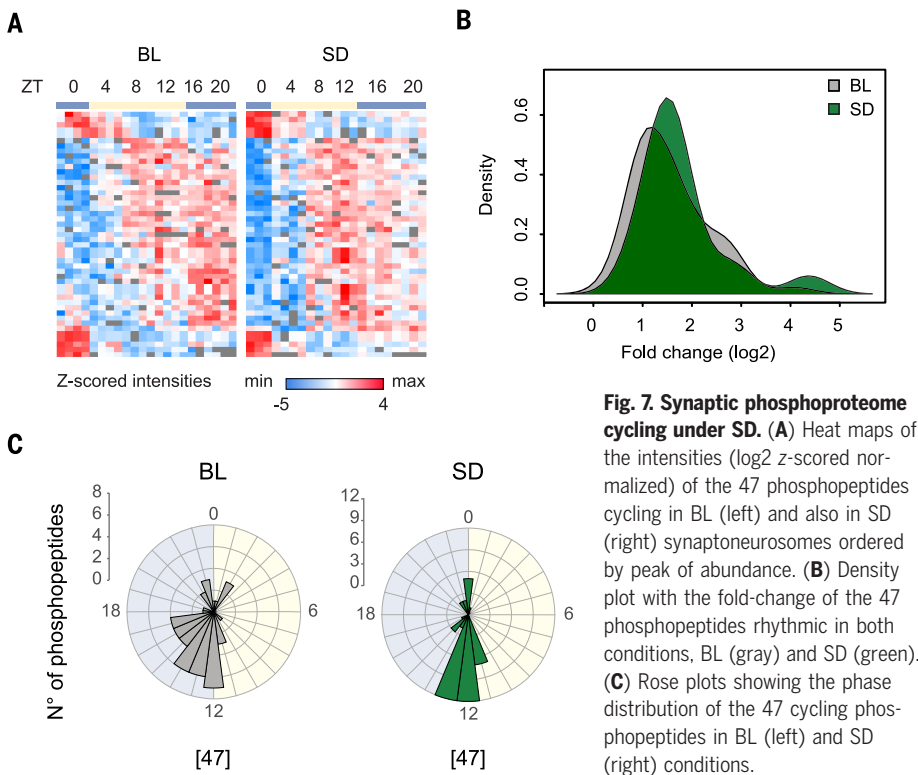
Fig. 7. Synaptic phosphoproteome cycling under SD. (**A**) Heat maps of the intensities (log2 z-scored normalized) of the 47 phosphopeptides cycling in BL (left) and also in SD (right) synaptoneurosomes ordered by peak of abundance. (**B**) Density plot with the fold-change of the 47 phosphopeptides rhythmic in both conditions, BL (gray) and SD (green). (**C**) Rose plots showing the phase distribution of the 47 cycling phosphopeptides in BL (left) and SD (right) conditions.

replicate 1 of ZT0, 4 of ZT8, and 2 of ZT12 of the sleep deprived group.

Bioinformatic and statistical analyses

Processed data was uploaded in the Perseus software (*14*) to perform bioinformatical analyses. First, reverse sequences and potential contaminants were removed from the total matrix. Then phosphopeptides intensities were log2 transformed and after expanding the site table, phosphopeptide entries without intensities in <12 samples independently in each data set (SD/BL) were removed. Following this, a normalization was applied to each sample individually: the intensity of every phosphopeptide was divided by the median intensity of all phosphopeptides in the same sample. Relative enrichment of UniProt KB -Keywords annotations in the total BL phosphoproteome dataset was achieved using Fisher's exact test enrichment analyses (FDR < 0.02) comparing to a total in silico mouse gene list generated by Perseus, both datasets were matched using gene names. Cycling analyses were performed as described using the computational platform Perseus (*2*, *14*). Phosphopeptides with a q < 0.05 were classified as "cycling." Hierarchical clustering was performed in a phase preserving-manner by which the order of elements is restricted to that determined by the output of the periodicity analysis. The proteome and the phosphoproteome data were matched using Uniprot ID. Amplitudes were calculated as the difference between maximum and minimum values across all the time points using the mean

of log2 intensities for the biological replicates. Cycling phosphopeptides were divided in two groups depending on their peak of phosphorylation ("phase"): one group containing phosphopeptides which peak between ZT18 to ZT6 and the other group comprising phosphopeptides which peak between ZT6 to ZT18. Relative enrichment of UniProt KB -Keywords annotations for both groups was individually performed using Fisher's exact test enrichment analyses (P < 0.05) comparing the protein annotations of both groups to the protein annotations of the total cycling phosphopeptides.

Phosphopeptides belonging to kinases and phosphatases (using Keyword and manual annotations) were extracted from the total list of phosphopeptides and collapsed to protein entries (kinases). Kinases and phosphatases with at least one cycling phosphopeptide (cycling analysis, q < 0.05) were defined as "cycling." Gene name lists of all quantified kinases and of cycling kinases were submitted to www.kinhub.org to annotate kinases to the major families and to generate the kinase trees. Percentages of total quantified and cycling kinases in each family were calculated based on the entries for each family designated in www.kinhub.org.

Integrated analysis and visualization of phosphoproteomic data and protein-protein interaction network

Interactions for mouse were downloaded from STRING (v10.5) and filtered for high-confidence edges with scores of at least 0.9. Since the

node identifiers in the network are Ensemble protein IDs (ENSP), the protein groups in the phosphoproteomics data were mapped ENSP IDs using the UniProt annotations in Perseus. After annotating the nodes of the network with the data, signaling functionality scores were calculated using PHOTON. In brief, for each protein in the network a moderated *t* test was performed on the phosphorylation found on its neighbors in the network. Using a permutation-based FDR approach the resulting *P* value was corrected for multiple testing and transformed into a final score. Intuitively, proteins with high/low scores pro-/demote the phosphorylation of their neighbors. Cycling analysis was performed on the PHOTON scores to identify kinases with an oscillatory signaling functionality score (*q* < 0.05, period 24 hours). For the visualization, all cycling kinases and their interactions were extracted from the network. The subnetwork was overlaid with phosphorylation data from cycling sites and plotted using the d3.js library and manual layouting.

For the KSEA prediction, 1,664 site-specific mouse kinase substrate interactions were downloaded from phosphosite.org (*44*). The 7257 phosphopeptides could be mapped to 84 distinct kinase-substrate interactions. KSEA z-scores were calculated for all kinases in the network (*17*, *18*), resulting in 37 kinase activity profiles with at least 3 valid values. After z-scoring the profiles, periodicity analysis was performed and cycling (*q* < 0.05, period 24 hours) kinase activity profiles were visualized in a scatter plot.

Western blotting and antibodies

Synaptoneurosome lysates were loaded onto 4 to 12% Bis-Tris NuPAGE gels (Thermo Fisher Scientific). After electrophoreses proteins were transferred to a nitrocellulose membrane and blocked in 5% BSA in TBS with 0.1% Tween-20 for 1 hour at room temperature. The incubation with the primary antibody was done overnight at 4°C following supplier instructions. Antibodies were obtained from Cell Signaling: CAMKII pT286 (12716), GSK3β pS9 (5558), and PKC pS660 (9371). The same secondary antibody against rabbit was used for all phospho-specific antibodies (GE Healthcare, NA934V) and was incubated for 1 hour at RT. Loading control was done with an antibody against glyceraldehyde-3-phosphate dehydrogenase (GAPDH) conjugated with horseradish peroxidase from ThermoFisher Scientific (MA5-15738-HRP). Densitometric quantification was performed using the ImageJ software.

REFERENCES AND NOTES

1. D. Mauvoisin *et al.*, Circadian clock-dependent and -independent rhythmic proteomes implement distinct diurnal functions in mouse liver. *Proc. Natl. Acad. Sci. U.S.A.* **111**, 167–172 (2014). doi: 10.1073/pnas.1314066111; pmid: 24344304

2. M. S. Robles, J. Cox, M. Mann, In-vivo quantitative proteomics reveals a key contribution of post-transcriptional mechanisms to the circadian regulation of liver metabolism. *PLOS Genet.* **10**, e1004047 (2014). doi: 10.1371/journal.pgen.1004047; pmid: 24391516

3. M. S. Robles, S. J. Humphrey, M. Mann, Phosphorylation is a central mechanism for circadian control of metabolism and physiology. *Cell Metab.* **25**, 118–127 (2017). doi: 10.1016/j.cmet.2016.10.004; pmid: 27818261

4. F. Hosp, M. Mann, A primer on concepts and applications of proteomics in neuroscience. *Neuron* **96**, 558–571 (2017). doi: 10.1016/j.neuron.2017.09.025; pmid: 29096073

5. K. Sharma *et al.*, Cell type- and brain region-resolved mouse brain proteome. *Nat. Neurosci.* **18**, 1819–1831 (2015). doi: 10.1038/nn.4160; pmid: 26523646

6. J. J. Liu *et al.*, In vivo brain GPCR signaling elucidated by phosphoproteomics. *Science* **360**, eaao4927 (2018). doi: 10.1126/science.aao4927; pmid: 29930108

7. D. C. Dieterich, M. R. Kreutz, Proteomics of the synapse–A quantitative approach to neuronal plasticity. *Mol. Cell. Proteomics* **15**, 368–381 (2016). doi: 10.1074/mcp.R115.051482; pmid: 26307175

8. K. M. Woolfrey, M. L. Dell'Acqua, Coordination of protein phosphorylation and dephosphorylation in synaptic plasticity. *J. Biol. Chem.* **290**, 28604–28612 (2015). doi: 10.1074/jbc.R115.657262; pmid: 26453308

9. G. H. Diering *et al.*, Homer1a drives homeostatic scaling-down of excitatory synapses during sleep. *Science* **355**, 511–515 (2017). doi: 10.1126/science.aai8355; pmid: 28154077

10. Z. Wang *et al.*, Quantitative phosphoproteomic analysis of the molecular substrates of sleep need. *Nature* **558**, 435–439 (2018). doi: 10.1038/s41586-018-0218-8; pmid: 29899451

11. S. B. Noya *et al.*, The forebrain synaptic transcriptome is organized by clocks, but its proteome is driven by sleep. *Science* **366**, eaav2642 (2019).

12. P. R. Dunkley, P. E. Jarvie, P. J. Robinson, A rapid Percoll gradient procedure for preparation of synaptosomes. *Nat. Protoc.* **3**, 1718–1728 (2008). doi: 10.1038/nprot.2008.171; pmid: 18927557

13. S. J. Humphrey, S. B. Azimifar, M. Mann, High-throughput phosphoproteomics reveals in vivo insulin signaling dynamics. *Nat. Biotechnol.* **33**, 990–995 (2015). doi: 10.1038/nbt.3327; pmid: 26280412

14. S. Tyanova *et al.*, The Perseus computational platform for comprehensive analysis of (prote)omics data. *Nat. Methods* **13**, 731–740 (2016). doi: 10.1038/nmeth.3901; pmid: 27348712

15. K. O. Lai, Z. Liang, E. Fei, H. Huang, N. Y. Ip, Cyclin-dependent kinase 5 (Cdk5)-dependent phosphorylation of p70 ribosomal S6 kinase 1 (S6K) is required for dendritic spine morphogenesis. *J. Biol. Chem.* **290**, 14637–14646 (2015). doi: 10.1074/jbc.M114.627117; pmid: 25903132

16. V. M. Ho, J. A. Lee, K. C. Martin, The cell biology of synaptic plasticity. *Science* **334**, 623–628 (2011). doi: 10.1126/science.1209236; pmid: 22053042

17. J. D. Rudolph, M. de Graauw, B. van de Water, T. Geiger, R. Sharan, Elucidation of signaling pathways from large-scale phosphoproteomic data using protein interaction networks. *Cell Syst.* **3**, 585–593.e3 (2016). doi: 10.1016/j.cels.2016.11.005; pmid: 28009266

18. P. Casado *et al.*, Kinase-substrate enrichment analysis provides insights into the heterogeneity of signaling pathway activation in leukemia cells. *Sci. Signal.* **6**, rs6 (2013). doi: 10.1126/scisignal.2003573; pmid: 23532336

19. L. M. Keranen, E. M. Dutil, A. C. Newton, Protein kinase C is regulated in vivo by three functionally distinct phosphorylations. *Curr. Biol.* **5**, 1394–1403 (1995). doi: 10.1016/S0960-9822(95)00277-6; pmid: 8749392

20. J. Lisman, R. Yasuda, S. Raghavachari, Mechanisms of CaMKII action in long-term potentiation. *Nat. Rev. Neurosci.* **13**, 169–182 (2012). doi: 10.1038/nrn3192; pmid: 22334212

21. C. A. Bradley *et al.*, A pivotal role of GSK-3 in synaptic plasticity. *Front. Mol. Neurosci.* **5**, 13 (2012). doi: 10.3389/fnmol.2012.00013; pmid: 22363262

22. D. A. Cross, D. R. Alessi, P. Cohen, M. Andjelkovich, B. A. Hemmings, Inhibition of glycogen synthase kinase-3 by insulin mediated by protein kinase B. *Nature* **378**, 785–789 (1995). doi: 10.1038/378785a0; pmid: 8524413

23. T. M. Thornton *et al.*, Phosphorylation by p38 MAPK as an alternative pathway for GSK3beta inactivation. *Science* **320**, 667–670 (2008). doi: 10.1126/science.1156037; pmid: 18451303

24. E. Shin *et al.*, Doublecortin-like kinase enhances dendritic remodelling and negatively regulates synapse maturation. *Nat. Commun.* **4**, 1440 (2013). doi: 10.1038/ncomms2443; pmid: 23385585

25. X. Xiao, A. D. Levy, B. J. Rosenberg, M. J. Higley, A. J. Koleske, Disruption of coordinated presynaptic and postsynaptic maturation underlies the defects in hippocampal synapse stability and plasticity in Abl2/Arg-deficient mice. *J. Neurosci.* **36**, 6778–6791 (2016). doi: 10.1523/JNEUROSCI.4092-15.2016; pmid: 27335408

26. C. Cirelli, C. M. Gutierrez, G. Tononi, Extensive and divergent effects of sleep and wakefulness on brain gene expression. *Neuron* **41**, 35–43 (2004). doi: 10.1016/S0896-6273(03)00814-6; pmid: 14715133

27. V. V. Vyazovskiy, C. Cirelli, M. Pfister-Genskow, U. Faraguna, G. Tononi, Molecular and electrophysiological evidence for net synaptic potentiation in wake and depression in sleep. *Nat. Neurosci.* **11**, 200–208 (2008). doi: 10.1038/nn2035; pmid: 18204445

28. I. Tobler, T. Deboer, M. Fischer, Sleep and sleep regulation in normal and prion protein-deficient mice. *J. Neurosci.* **17**, 1869–1879 (1997). doi: 10.1523/JNEUROSCI.17-05-01869.1997; pmid: 9030645

29. S. Maret *et al.*, Homer1a is a core brain molecular correlate of sleep loss. *Proc. Natl. Acad. Sci. U.S.A.* **104**, 20090–20095 (2007). doi: 10.1073/pnas.0710131104; pmid: 18077435

30. P. Franken, D. Chollet, M. Tafti, The homeostatic regulation of sleep need is under genetic control. *J. Neurosci.* **21**, 2610–2621 (2001). doi: 10.1523/JNEUROSCI.21-08-02610.2001; pmid: 11306614

31. N. Z. Gerges *et al.*, Independent functions of hsp90 in neurotransmitter release and in the continuous synaptic cycling of AMPA receptors. *J. Neurosci.* **24**, 4758–4766 (2004). doi: 10.1523/JNEUROSCI.0594-04.2004; pmid: 15152036

32. D. Ivanova, A. Dirks, A. Fejtova, Bassoon and piccolo regulate ubiquitination and link presynaptic molecular dynamics with activity-regulated gene expression. *J. Physiol.* **594**, 5441–5448 (2016). doi: 10.1113/JP271826; pmid: 26915533

33. J. Li *et al.*, Long-term potentiation modulates synaptic phosphorylation networks and reshapes the structure of the postsynaptic interactome. *Sci. Signal.* **9**, rs8 (2016). doi: 10.1126/scisignal.aaf6716; pmid: 27507650

34. G. Tononi, C. Cirelli, Sleep and the price of plasticity: From synaptic and cellular homeostasis to memory consolidation and integration. *Neuron* **81**, 12–34 (2014). doi: 10.1016/j.neuron.2013.12.025; pmid: 24411729

35. L. L. Baltussen, F. Rosianu, S. K. Ultanir, Kinases in synaptic development and neurological diseases. *Prog. Neuropsychopharmacol. Biol. Psychiatry* **84**, 343–352 (2018). doi: 10.1016/j.pnpbp.2017.12.006; pmid: 29241837

36. C. Hooper *et al.*, Glycogen synthase kinase-3 inhibition is integral to long-term potentiation. *Eur. J. Neurosci.* **25**, 81–86 (2007). doi: 10.1111/j.1460-9568.2006.05245.x; pmid: 17241269

37. G. Tononi, C. Cirelli, Sleep function and synaptic homeostasis. *Sleep Med. Rev.* **10**, 49–62 (2006). doi: 10.1016/j.smrv.2005.05.002; pmid: 16376591

38. R. Iyer, T. A. Wang, M. U. Gillette, Circadian gating of neuronal functionality: A basis for iterative metaplasticity.

39. V. Mongrain *et al.*, Separating the contribution of glucocorticoids and wakefulness to the molecular and electrophysiological correlates of sleep homeostasis. *Sleep* **33**, 1147–1157 (2010). doi: 10.1093/sleep/33.9.1147; pmid: 20857860

40. A. Balsalobre *et al.*, Resetting of circadian time in peripheral tissues by glucocorticoid signaling. *Science* **289**, 2344–2347 (2000). doi: 10.1126/science.289.5488.2344; pmid: 11009419

41. S. A. Brown, G. Zumbrunn, F. Fleury-Olela, N. Preitner, U. Schibler, Rhythms of mammalian body temperature can sustain peripheral circadian clocks. *Curr. Biol.* **12**, 1574–1583 (2002). doi: 10.1016/S0960-9822(02)01145-4; pmid: 12372249

42. I. Tobler, K. Jaggi, Sleep and EEG spectra in the Syrian hamster (*Mesocricetus auratus*) under baseline conditions and following sleep deprivation. *J. Comp. Physiol. A* **161**, 449–459 (1987). doi: 10.1007/BF00603970; pmid: 3668881

43. S. Tyanova, T. Temu, J. Cox, The MaxQuant computational platform for mass spectrometry-based shotgun proteomics. *Nat. Protoc.* **11**, 2301–2319 (2016). doi: 10.1038/nprot.2016.136; pmid: 27809316

44. P. V. Hornbeck *et al.*, PhosphoSitePlus, 2014: Mutations, PTMs and recalibrations. *Nucleic Acids Res.* **43**, D512–D520 (2015). doi: 10.1093/nar/gku1267; pmid: 25514926

45. J. A. Vizcaíno *et al.*, 2016 update of the PRIDE database and its related tools. *Nucleic Acids Res.* **44**, D447–D456 (2016). doi: 10.1093/nar/gkv1145; pmid: 26527722

SUPPLEMENTARY MATERIALS

science.sciencemag.org/content/366/6462/eaav3617/suppl/DC1
Figures S1 to S13
Tables S1 to S6
View/request a protocol for this paper from *Bio-protocol*.

Science

Sleep-wake cycles drive daily dynamics of synaptic phosphorylation

Franziska Brüning, Sara B. Noya, Tanja Bange, Stella Koutsouli, Jan D. Rudolph, Shiva K. Tyagarajan, Jürgen Cox, Matthias Mann, Steven A. Brown and Maria S. Robles

Sleep-wake cycles at mouse synapses
Analysis of the transcriptome, proteome, and phosphoproteome at synapses in the mouse brain during daily sleep-wake cycles reveals large dynamic changes (see the Perspective by Cirelli and Tononi). Noya *et al.* found that almost 70% of transcripts showed changes in abundance during daily circadian cycles. Transcripts and proteins associated with synaptic signaling accumulated before the active phase (dusk for these nocturnal animals), whereas messenger RNAs and protein associated with metabolism and translation accumulated before the resting phase. Brüning *et al.* found that half of the 2000 synaptic phosphoproteins quantified showed changes with daily activity-rest cycles. Sleep deprivation abolished nearly all (98%) of these phosphorylation cycles at synapses.
Science, this issue p. eaav2642, p. eaav3617; see also p. 189

ARTICLE TOOLS	http://science.sciencemag.org/content/366/6462/eaav3617
SUPPLEMENTARY MATERIALS	http://science.sciencemag.org/content/suppl/2019/10/09/366.6462.eaav3617.DC1
RELATED CONTENT	http://science.sciencemag.org/content/sci/366/6462/189.full http://science.sciencemag.org/content/sci/366/6462/eaav5728.full http://stm.sciencemag.org/content/scitransmed/11/474/eaau6550.full http://stm.sciencemag.org/content/scitransmed/5/179/179ra44.full http://stm.sciencemag.org/content/scitransmed/4/150/150ra122.full http://stm.sciencemag.org/content/scitransmed/4/129/129ra43.full
REFERENCES	This article cites 45 articles, 17 of which you can access for free http://science.sciencemag.org/content/366/6462/eaav3617#BIBL
PERMISSIONS	http://www.sciencemag.org/help/reprints-and-permissions

Use of this article is subject to the Terms of Service